

Stable and unstable vortices attached to seamounts

By J. NYCANDER¹ AND J. H. LACASCE²

¹Stockholm University, Department of Meteorology, Stockholm, Sweden

²Norwegian Meteorological Institute, Oslo, Norway

(Received 1 April 2003 and in revised form 22 December 2003)

We examine the properties of stationary, barotropic flows over isolated topographic features such as seamounts. According to a general variational principle, flows that maximize or minimize the energy in a set of isovortical flows are stationary and stable. Using this, it is shown that a large class of stable and stationary attached anticyclones exists at a seamount. Those with positive potential vorticity (PV) are maximum energy states, while those with negative PV are minimum energy states. If the seamount is circular, there are also stable attached cyclones, but these are destabilized by irregularities in the topographic shape, unlike the anticyclones. Numerical simulations broadly support these theoretical predictions, but also highlight the importance of time-dependent processes, particularly in cases in which the vortex collides with the seamount.

1. Introduction

There is a long-standing interest in flow over isolated topography, such as seamounts, with regard to both theoretical and practical issues. Trapped flows are often observed over seamounts, and these flows evidently affect the distribution and concentration of subsurface fauna, filter feeders and the like (e.g. Genin, Noble & Lonsdale 1989 and references therein). These flows are often so intense that they alter the ambient vorticity and, as such, can modify the allowable frequencies of internal waves. This in turn may affect wave breaking (Kunze & Toole 1997 and references therein).

Seamount-trapped flows are usually explained in terms of Taylor–Proudman dynamics (e.g. Taylor 1917). Flow past an isolated obstacle in a rotating fluid is diverted around the obstacle and generates a region of trapped circulation over it (Greenspan 1968). If the ambient flow has zero potential vorticity (PV), the trapped ‘Taylor column’ or ‘cap’ likewise has zero PV. In a stratified fluid, the column is bottom-trapped, possessing a vertical scale which varies with the Burgers number associated with the bump (e.g. Hogg 1973). A Taylor cap has anticyclonic flow, and this is generally the sense of the observed seamount-trapped currents.

There are other theories which also predict trapped flow over isolated topography. Statistical mechanics predicts that the state of maximum entropy in a random two-dimensional flow over topography has a non-zero mean which is anticorrelated with the topography, yielding an anticyclonic flow over a seamount (Salmon, Holloway & Hendershott 1976). Variational arguments suggest that such a flow also minimizes enstrophy (squared vorticity) (Bretherton & Haidvogel 1976), a pertinent point given that enstrophy cascades to small scales and is dissipated in two-dimensional turbulence. The solutions obtained with this approach are the same as the mean flow predicted by the statistical mechanics theory in the limit of infinite resolution (Carnevale & Frederiksen 1987, referred to as CF hereinafter).

With bottom friction, oscillating flow over an obstacle can drive a rectified flow like a Taylor cap. Such ‘tidal rectification’ (Zimmerman 1978; Loder 1980) is a forced-dissipative phenomenon and is to be distinguished from the inviscid or nearly inviscid solutions above. Nevertheless, it is often invoked to explain anticyclonic flows over seamounts.

The present work falls into the category of the inviscid theory. According to a classical variational principle, a flow that maximizes or minimizes the energy in a set of isovortical flows is stationary and stable (Arnol’d 1978). (‘Isovortical flows’ will be defined in §2; essentially, their PV fields can be made identical by some incompressible deformation.) This variational principle was generalized by Johnson (1978) to geophysical flows with topography.

Here we use a special case of Johnson’s principle, where we restrict attention to small-amplitude topography (i.e. the quasi-geostrophic limit), and to flow that is quiescent at infinity. We use it to prove the existence of a large family of stable monopole vortices attached to a given localized topographic anomaly. Some of these flows are global energy maxima, and some global minima. The attached dipole vortex solutions found numerically by Johnson (1978), by contrast, are local maxima.

Note that we use the full set of invariants, including the isovortical constraint. This is the main difference to the variational approach of Bretherton & Haidvogel (1976) and CF, who used only the quadratic invariants. We therefore find a larger set of stationary and stable flows, which includes both Taylor caps and the solutions found by CF as subsets.

Finally, we want to mention a different variational principle proposed by Shnirelman (1993). It seems to be capable of giving other stationary solutions than those given by the variational principle used here, although the relation between the two different principles is not clear to us.

In addition to the theory, we present results from numerical simulations. These are done in order to examine whether the predicted stable flows can arise naturally as a result of the time-dependent evolution. As the initial condition, we use various non-stationary vortices near or on top of a seamount. We also revisit two-dimensional turbulence over a bump. The simulations are broadly supportive of the theoretical predictions, although time-dependence can produce exotic and interesting final states.

2. Theory

2.1. Conservation laws and variational principle

The basic equation used in the present work is the barotropic vorticity equation,

$$\frac{\partial}{\partial t} \nabla^2 \phi + J(\phi, \nabla^2 \phi + h) = 0, \quad (1)$$

where ϕ is the streamfunction and J denotes the Jacobian: $J(f, g) \equiv \partial_x f \partial_y g - \partial_y f \partial_x g$. This equation describes the Lagrangian conservation of PV, i.e. $dq/dt = 0$. The PV is defined by

$$q \equiv \omega + h(\mathbf{r}), \quad (2)$$

where $\omega = \nabla^2 \phi$ is the relative vorticity, and $h(\mathbf{r})$ is the height of the bottom topography relative to a constant background value. We will study a localized topographic feature on an infinite plane.

The total energy of a flow is given by $(1/2) \int (\nabla \phi)^2 d\mathbf{r}$. However, this is infinite for two-dimensional flows with non-zero circulation, and it is therefore customary to

replace it by the conserved and finite integral E , defined by

$$\begin{aligned} E &= -\frac{1}{2} \int \omega \phi \, d\mathbf{r} \\ &= -\frac{1}{4\pi} \int \int [q(\mathbf{r}) - h(\mathbf{r})][q(\mathbf{r}') - h(\mathbf{r}')]\ln|\mathbf{r} - \mathbf{r}'| \, d\mathbf{r} \, d\mathbf{r}', \end{aligned} \quad (3)$$

which can also be written as

$$E = -\frac{1}{4\pi} \int \int q(\mathbf{r})q(\mathbf{r}')\ln|\mathbf{r} - \mathbf{r}'| \, d\mathbf{r} \, d\mathbf{r}' + \int q\eta \, d\mathbf{r} - \frac{1}{2} \int h\eta \, d\mathbf{r}, \quad (4)$$

where we defined

$$\eta(\mathbf{r}) = \frac{1}{2\pi} \int h(\mathbf{r}')\ln|\mathbf{r} - \mathbf{r}'| \, d\mathbf{r}', \quad (5)$$

so that

$$\nabla^2 \eta = h. \quad (6)$$

Note that the last term of (4) is independent of q .

Physically, E represents that part of the total energy which depends on the way in which the given total amount of vorticity is distributed. Effectively, an infinite constant has been subtracted from the total energy. It would perhaps be appropriate to call E the ‘excess energy’, but we will (like many other authors) simply call it the ‘energy’.

The energy E is conserved regardless of the shape of the seamount. If, however, the seamount is circularly symmetric, i.e. $h = h(r)$, equation (1) in addition conserves the angular momentum M :

$$M = \int q r^2 \, d\mathbf{r}. \quad (7)$$

(The real angular momentum is infinite, but although M should perhaps be called the ‘excess angular momentum’, we will use the simpler ‘angular momentum’.) Equation (1) also conserves an infinite family of Casimir integrals:

$$C_F = \int F[q(\mathbf{r})] \, d\mathbf{r}, \quad (8)$$

where F is an arbitrary function. Flows that have the same value of all the Casimir integrals are called isovortical flows, and perturbations of the PV-field that keep the flow in the same set of isovortical flows are said to be isovortical perturbations. Also, fields $q(\mathbf{r})$ in the same set of isovortical flows are said to be rearrangements of each other. A rearrangement can be thought of as an incompressible deformation.

According to a general variational principle, flows that satisfy $\delta E = 0$ for arbitrary isovortical perturbations are stationary, i.e. satisfy $J(\phi, q) \equiv 0$ (Arnol’d 1978). This can be demonstrated by noting that a general first-order isovortical perturbation of a given field $q(\mathbf{r})$ (i.e. a perturbation that satisfies $\delta C_F = 0$ for any F) is given by $\delta q = J(\xi, q)$, where $\xi(\mathbf{r})$ is arbitrary. The corresponding energy variation is

$$\delta E = - \int \phi \delta q \, d\mathbf{r} = \int \xi J(\phi, q) \, d\mathbf{r}, \quad (9)$$

which gives the desired result.

Moreover, if a stationary point of the energy integral is an extremum (using the isovortical constraint), the flow is stable, analogously to Lyapunov stability for a system with a finite number of degrees of freedom. Thus, stability is related to energy

variations of higher order. Isovortical perturbations to all orders are given by the Lie series

$$\Delta q = \delta q + \frac{1}{2}\delta^2 q + \dots = J(\xi, q) + \frac{1}{2}J(\xi, J(\xi, q)) + \dots \quad (10)$$

The second-order energy variation is

$$\delta^2 E = -\frac{1}{4\pi} \int \int [\delta\omega(\mathbf{r})\delta\omega(\mathbf{r}') + \delta^2\omega(\mathbf{r})\omega(\mathbf{r}')] \ln|\mathbf{r} - \mathbf{r}'| \, d\mathbf{r} \, d\mathbf{r}'.$$

Using (10) and the fact that $\delta q = \delta\omega = \nabla^2\delta\phi$ this can be rewritten as

$$\begin{aligned} \delta^2 E &= -\frac{1}{2} \int (\delta\phi\delta q + \phi\delta^2 q) \, d\mathbf{r} \\ &= -\frac{1}{2} \int [\delta\phi\delta q - J(\xi, \phi)J(\xi, q)] \, d\mathbf{r} \\ &= \frac{1}{2} \int \left[-\delta\phi\delta q + \frac{d\phi}{dq}(\delta q)^2 \right] \, d\mathbf{r}, \end{aligned} \quad (11)$$

where we assumed that the flow is stationary, so that ϕ and q are functionally related.

If δq and $\delta\phi$ are replaced by the first-order perturbations $q_1(\mathbf{r}, t)$ and $\phi_1(\mathbf{r}, t)$, $\delta^2 E$ becomes the ‘Arnol’d invariant’ A , which is conserved by the linearized equations about any stationary flow. Arnol’d (1966) showed that if $d\phi/dq \geq c > 0$ everywhere for some positive constant c , then the flow is nonlinearly stable, in the sense that an *a priori* estimate of a norm can be given. (This is usually referred to as ‘Arnol’d stability’.) In this case, A is positive definite for arbitrary ϕ_1 .

For a minimum energy flow, i.e. a flow that minimizes E in a set of isovortical flows, $\delta^2 E$ must be positive for any isovortical perturbation δq . By choosing a localized δq with small enough spatial scale, we can make the second term in (11) dominant, and $d\phi/dq$ must therefore be positive everywhere. Hence, a minimum energy flow is Arnol’d stable.

For a maximum energy flow, $\delta^2 E$ must be negative for any isovortical perturbation δq , which implies that $d\phi/dq$ is negative everywhere. However, $d\phi/dq$ being negative is not a sufficient condition for Arnol’d stability, since the first term in (11) is positive. In fact, on an infinite plane it is, in general, possible to find a perturbation ϕ_1 for which A is positive, even if $d\phi/dq$ is negative (Nycander 2003). Thus, $\delta^2 E$ is negative for any isovortical perturbations, but not for arbitrary non-isovortical perturbations.

A maximum energy flow on an infinite plane is therefore not Arnol’d stable. However, it is linearly stable (Nycander 1995). Also, the strongest nonlinear instability, the explosive resonant interaction, is prevented, since it requires the existence of isovortical perturbations with opposite signs of $\delta^2 E$ (Vanneste 1995). A maximum energy flow is therefore nonlinearly stable in a practical sense, as also argued by Benjamin (1976), but this cannot be formalized to a statement of stability in some norm.

We will not here try to prove sign definiteness of $\delta^2 E$ directly, as in Arnol’d stability. Rather, we will show the existence of a global energy maximum or minimum. By implication, the corresponding flow is stationary and stable, and $\delta^2 E$ is sign definite for isovortical perturbations. A similar approach has been used to show the existence of stationary vortex rings and dipole vortices (Benjamin 1976; Burton 1987, 1988). It has also been used to show the existence of a large class of stationary and stable localized vortices in a uniform background shear flow, both for two-dimensional flow (Nycander 1995; Emamizadeh 2000) and three-dimensional quasi-geostrophic flow

(Burton & Nycander 1999). This was done by proving the existence of a maximum energy flow. In the present case, the approach will be used to understand the dynamics of vortices attached to seamounts. We will show the existence of both maximum energy flows and minimum energy flows.

2.2. Flat topography or circular seamount

We begin with the simple uniform case, i.e. $h \equiv 0$. In this case, any circular vortex with a monotonic PV-profile is a maximum energy flow, and therefore stable, as is well known. To see this, we use an argument from Filippov & Yan'kov (1986), and think of q as the density of some incompressible fluid. If we change the sign of (4) and set $\eta \equiv 0$, the right-hand side has exactly the same form as the potential energy owing to two-dimensional attractive gravitational forces. If q has only one sign, it is intuitively obvious that the minimum potential energy (i.e. the maximum of E) is attained by a circular distribution with the densest matter in the centre, the two-dimensional counterpart of the density structure of planets and stars. This can also be rigorously proved with the help of theorems about symmetrizations (Sobolev 1963).

Alternatively, stability can be proved by using the conservation of angular momentum. Equation (7) can be interpreted as the potential energy of the density distribution $q(\mathbf{r})$ in an external potential well proportional to r^2 . The minimum of M (or the maximum, if q is negative) is then obviously attained by a circular vortex with monotonic PV-profile. Again, the conclusion is that such a vortex is stable.

The latter argument also holds without any change in the presence of a circular seamount, since the angular momentum is not affected by circularly symmetric topography. Hence, any circular vortex (cyclone or anticyclone) which has a monotonic PV-profile and is centred on a circular seamount is stable.

2.3. Irregular seamount

We now assume that there is a localized seamount, satisfying

$$\int h \, d\mathbf{r} = H < \infty.$$

For simplicity, we assume that the support of h (i.e. the region where $h \neq 0$) is bounded, and that $h \geq 0$. (Note that (1) is invariant to changing the sign of h , ϕ and either x or y , so that a cyclone over a seamount is equivalent to an anticyclone over a depression.) There are no other restrictions on the shape of the seamount. The function $\eta(\mathbf{r})$ defined in (5) then has a minimum at the seamount, and increases outward; we have $\eta \sim (H/2\pi)\ln(r)$ as $r \rightarrow \infty$.

The support of q is also assumed to be bounded, and q is assumed to have the same sign (either positive or negative) everywhere on its support.

An important solution in this case is given by $q(\mathbf{r}) \equiv 0$. This is the anticyclonic Taylor cap, with the streamfunction given by $\phi = -\eta$, as can be seen from (2) and (6). Such a vortex is obviously stable. Indeed, from (1), we see that there is no dynamics at all, in the sense that no isovortical perturbations are possible: the set of isovortical flows contains no other flow.

We then assume that $q \leq 0$. As in the case with flat topography, the first term of (4) is maximized by placing fluid elements with large negative values of q as close to each other as possible. The second term is maximized by placing fluid elements with large negative values of q where η is small, so that the contour curves of η and q coincide. Thus, there is almost no conflict between the requirements for maximizing the two terms, and the maximum of the whole expression is clearly attained by a localized

distribution of q with the minimum at the seamount, and q increasing toward zero outward. A rigorous proof of this has been given by Nycander & Emamizadeh (2003).

This proves the existence of a large class of stationary and stable anticyclonic vortices attached to a seamount. They are non-circular, unless $h(\mathbf{r})$ is circularly symmetric. The radial profile of q is in general monotonic, but otherwise arbitrary. (If the topography is very irregular, so that η has several minima, the profile of the maximizing field q may actually be non-monotonic, but q is still localized. In what follows, we will restrict ourselves to cases where η has only one minimum.) A vortex of this kind exists in every set of isovortical flows for which $q \leq 0$ everywhere. It rotates in the same direction as the Taylor cap, but faster. This set of vortex solutions is similar to the stationary and stable vortices that exist in a uniform background shear flow (Nycander 1995).

We then assume that $q \geq 0$. The second term of (4) is in this case maximized by placing fluid elements with large values of q as far away from the seamount as possible, while the first term is still maximized by placing these fluid elements as close to each other as possible. Clearly, the maximum is not attained by a vortex attached to the seamount.

Instead, we look for a minimum energy flow. To minimize the first term, we should spread out the fluid elements with $q > 0$ as much as possible, but to minimize the second term they should be placed at the seamount. Since these requirements are in conflict, the situation is more delicate than before, and depends on the relative strength of q and h .

A necessary condition for the existence of a minimum energy flow in this case is

$$\int_0^R q^* r \, dr \leq \int_0^R h^* r \, dr \quad (12)$$

for any $R > 0$. Here, q^* and h^* are the symmetrizations of q and h , respectively. (A symmetrization can be defined as the unique rearrangement which is circularly symmetric and monotonic decreasing outward from the origin.)

To show this, we recall that a minimum energy flow has $d\phi/dq \geq 0$ everywhere, as was pointed out in §2.1. Since ∇q must be directed inward in a localized vortex with $q \geq 0$, this means that $\nabla\phi$ is also directed inward. Using Gauss' theorem, we conclude that a minimum energy vortex satisfies $\int_S \omega \, d\mathbf{r} < 0$, where S is any region bounded by a streamline $\phi = \text{const}$. Since $\omega = q - h$, this in turn implies the condition (12), which is therefore a necessary condition for the existence of a minimum energy flow.

We have no rigorous proof that the condition (12) is also sufficient, but in the following we will present arguments to make it plausible.

An analogy with electrostatics is useful in this case, and (3) is the most appropriate form of the energy. If we interpret q as the density of free charges (positive), and $-h$ as the density of bound charges (negative) that are kept in place by some external forces, then E is the electrostatic energy and $-\phi$ the electrostatic potential. An electrostatic equilibrium corresponds to a minimum energy flow. In such electrostatic problems, the charges are usually assumed to be free to be distributed arbitrarily, without any upper bound on the charge density. This means that there are no Casimir constraints, only the constraint defined by the total free charge $Q = \int q \, d\mathbf{r}$.

If $Q > H$, the bound charges will be completely neutralized by the free charges at equilibrium, so that $q = h$ on the support of h , while the surplus charges will be repelled toward infinity. Thus, there is no localized minimum energy state.

If $Q \leq H$, on the other hand, all the free charges will be attracted by the bound charges, and at equilibrium they are all situated in a central region where $q = h$ and the electrostatic potential $-\phi$ is constant. The only non-trivial part of the solution is to find the boundary of this region.

Adding the Casimir constraints to this picture corresponds to q being the charge density of some incompressible fluid. Assume first that the inequality (12) is reversed for some $R = R_0$. Assume also that the region where $q > q^*(R_0)$ is a simply connected region, and apply Gauss' theorem to the integral of $\nabla^2 \phi = q - h$ over this region. We find that the gradient of the electrostatic potential $-\phi$ at the bounding curve is on average directed inward (i.e. the electrostatic force on the free charges is outward). This is clearly impossible at equilibrium, which agrees with the conclusion above that (12) is a necessary condition. The equilibrium is instead attained by mixing fluid particles with different values of q , 'diluting' the free charges. In this way, the effective charge density \bar{q} (the average of q over small scales) can be decreased until the condition (12) is satisfied by \bar{q} , provided that $Q \leq H$. Thus, a sequence of rearrangements q_n for which $E[q_n]$ approaches the minimum value will be more and more filamented, and no minimum exists in the set of rearrangements. (However, it does exist in the closed convex hull of this set, to which \bar{q} belongs (Burton & Nycander 1999).)

If, on the other hand, the condition (12) is satisfied, the free charges are unable to neutralize the bound charges, so that even when they are closely packed, the gradient of the electrostatic potential $-\phi$ is directed outward, i.e. $d\phi/dq$ is positive. In this case, an electrostatic equilibrium exists, and hence a minimum energy flow. This flow is Arnol'd stable.

We have no mathematical proof that the condition (12) is sufficient for the existence of a minimum energy flow, but we believe the heuristic argument presented above to be convincing. Moreover, the conclusions will be supported by numerical simulations.

From the condition $\int_S \omega \, d\mathbf{r} < 0$ implied by (12), it follows that the circulation along any streamline is anticyclonic. Thus, the minimum energy vortices are anticyclones, but, unlike the maximum energy vortices, they rotate more slowly than the Taylor cap.

We conclude that there exists a large set of stable anticyclonic vortex solutions over an arbitrarily shaped seamount, and they can be either maximum or minimum energy flows. Stable cyclones, on the other hand, only exist if the seamount is circular.

The present results give some properties of the stable flows, but not the explicit solutions. In most cases, these would have to be found numerically. A numerical method that would be well suited for this is the pseudo-advective relaxation employed by Carnevale & Vallis (1990). Essentially, this algorithm solves the variational problem considered here numerically, and the present results give a prescription of how to choose the initial condition for the relaxation procedure.

A related relaxation procedure was also used by Johnson (1978) to find stationary dipole vortices attached to a seamount in a uniform background flow. These solutions are local energy maxima rather than the global extrema considered here.

2.4. Comparison with the theory of Carnevale & Frederiksen

The present work is closely related to several earlier ones. Bretherton & Haidvogel (1976) used a variational approach to examine minimum enstrophy flows over topography, and Salmon *et al.* (1976) adopted a statistical mechanics approach to predict mean flows over topography in the presence of random two-dimensional

turbulence. These two theories were unified by CF. Let us therefore compare the present work with that of CF.

In the variational approach of CF, the only invariants were the energy and enstrophy. The latter is the same as the quadratic Casimir invariant, which is obtained by setting $F(q) = q^2$ in (8). CF moreover assumed the domain to be doubly periodic. Our theory is for a localized topographic feature on an infinite plane; however, their analysis can be adapted to the infinite plane.

CF considered stationary solutions of the form

$$\nabla^2 \phi + h = \mu \phi, \quad (13)$$

where μ is a constant. Define the wavenumber spectrum as all k^2 for which the homogeneous equation

$$\nabla^2 \phi = -k^2 \phi \quad (14)$$

has a non-trivial solution. If $-\mu$ belongs to this spectrum, (13) is singular. On a doubly periodic domain, the spectrum is discrete, and has a low wavenumber cutoff k_0^2 . CF also assumed that there is a high wavenumber cutoff k_1^2 due to finite resolution, as would be the case in a numerical simulation. Thus, the spectrum is confined to $k_0^2 < k^2 < k_1^2$. They then showed that solutions of the form (13) are Arnol'd stable if $\mu < -k_1^2$ or $\mu > -k_0^2$. (Note that the fact that $-\mu$ is outside the spectrum guarantees that (13) has a unique solution.) They did this by showing that these solutions minimize the energy if $\mu < -k_1^2$ or $\mu > 0$, and that they maximize the energy if $-k_0^2 < \mu < 0$, in all cases with the enstrophy kept fixed. (They also used an alternative but equivalent formulation, according to which these solutions maximize or minimize the enstrophy, with the energy kept fixed.)

At infinite resolution, the high-wavenumber cutoff goes to infinity, $k_1 \rightarrow \infty$, and on an infinite plane, the low-wavenumber cutoff goes to zero, $k_0 \rightarrow 0$. Moreover, the spectrum becomes continuous, and covers the whole range $0 < k^2 < \infty$. Thus, for this case, their theory shows that solutions to (13) are nonlinearly stable minimum energy flows if $\mu > 0$. These are also the values of μ for which (13) has a unique solution. How, then, do these flows correspond to our theory?

Suppose that h is positive and describes an isolated seamount with a single maximum point. Then, assuming that $\mu > 0$, the solution ϕ defined by (13) is positive, has a maximum at the seamount and goes to zero at infinity. (This can be seen by expressing the solution in terms of the Green's function.) Thus, this is an anticyclone. Moreover, from the relation $q = \mu \phi$, we find that $q > 0$. Thus, this anticyclone rotates more slowly than the Taylor cap, and corresponds to a minimum energy vortex in our theory.

Since the circulation along any streamline is anticyclonic, applying Gauss' theorem to the integral of (2) gives the inequality

$$\int_S q \, d\mathbf{r} < \int_S h \, d\mathbf{r}, \quad (15)$$

where S is the area inside any streamline. This implies that (12) is satisfied.

The solution of (13) decays exponentially as $r \rightarrow \infty$, i.e. it describes a 'shielded' vortex, in which a core of negative relative vorticity $\nabla^2 \phi$ is surrounded by a shield with positive relative vorticity. Hence, $q < h$ in the core, while $q > h$ in the shield. Integrating (2) over the whole plane, we obtain $Q = H$, where $Q = \int q \, d\mathbf{r}$. Thus, we are on the boundary of the necessary condition $Q \leq H$ found in our analysis.

We conclude that the stable solutions of CF correspond to minimum energy vortices in our theory. However, the maximum energy vortices in our theory have no counterpart in their theory, nor do the minimum energy vortices with $Q < H$, i.e. those which are unshielded or only partly shielded. In fact, even most of the shielded minimum energy vortices, satisfying $Q = H$, have no counterpart in their theory, since few sets of isovortical flows give a linear relation $q = \mu\phi$. The set where q is piecewise constant is one example which cannot give such a linear relation. So the flows of CF are a small subset of the stable solutions identified herein.

CF also considered solutions with a nonlinear relation between the PV and the streamfunction, instead of (13). In particular, they discussed the consequences of such solutions for the statistical mechanics theories. However, they did not try to characterize such nonlinear solutions or show that they exist, as has been done here.

3. Experiments

3.1. Model

The preceding considerations pertain to steady flows, but do not address the question of how such flows could arise. Furthermore, the arguments in support of the minimum energy vortex are not rigorous. To see which solutions might occur as a result of the flow evolution, we therefore conducted a series of numerical simulations. The initial conditions were rather idealized, for instance an isolated vortex and a seamount.

We thus used a numerical model to solve (1). The model is barotropic, quasi-geostrophic, doubly periodic and fully spectral and is described by Flierl, Malanotte-Rizzoli & Zabusky (1987). It employs a leap-frog time step with an occasional Euler step for stability. Advection is computed as described by Patterson & Orszag (1971), but without dealiasing (which produced identical results but with 50% longer integrations). Dealiasing is essential if we wish to conserve enstrophy; however, enstrophy is removed in the present simulations at small scales (see below).

We will examine two types of experiment, one with a single vortex and a second with an initially random (turbulent) field. The vortex runs were made with 128^2 Fourier modes (and hence grid points in real space). The results with 64^2 modes were in most instances very similar. Enstrophy was removed via an (spectral) exponential wavenumber cutoff filter. This removes small-scale vorticity, but is less corrosive to vorticity maxima than biharmonic friction (LaCasce 1998). Nevertheless, some biharmonic friction was used to smooth small scales for presentation purposes in the figures; biharmonic friction was not used, for example, when we needed to make quantitative comparisons of the circulation over a seamount (to reduce the possibility of viscous effects on the trapped vorticity). The turbulence runs were made with 256^2 modes and only the wavenumber filter. Runs made with only 128^2 modes produced qualitatively similar results.

3.2. Single vortices

We consider the vortex simulations first. In all of these, the initial condition was a circularly symmetric vortex; in general, only the seamount was altered. The experiments can be broken into four subgroups. The first two (denoted S#) use a symmetric seamount and a vortex initially either aligned or unaligned with the seamount, respectively; the two additional sets (A#) concern aligned and unaligned vortices over an asymmetric seamount. The symmetric seamount had a Gaussian profile with maximum height H ; the asymmetric seamount had a Gaussian profile in

Experiment	$H, r_x/r_y$	A	δx	Comments
S1	2.0, 0.3/0.3	2.0	0	Stable
S2	2.0, 0.3/0.3	-2.0	0	Stable
S3	2.0, 0.3/0.3	-2.0	0.3	Cap (AC) with C satellite
S4	2.0, 0.3/0.3	2.0	0.3	C satellite
S5	2.0, 0.3/0.3	-2.0	0.6	Cap (AC) with dipole
S6	2.0, 0.3/0.3	2.0	0.6	C satellite, perturbed
A1	2.0, 0.6/0.3	-2.0	0	Cap (AC), stable
A2	2.0, 0.6/0.3	2.0	0	Fission, 2 C satellites
A3	2.0, 0.6/0.3	-2.0	0.3	Cap (AC), C satellite
A4	2.0, 0.6/0.3	2.0	0.3	Fission, 2 C satellites
A5	2.0, 0.6/0.3	-2.0	0.6	Cap (AC), C satellite
A6	2.0, 0.6/0.3	2.0	0.6	C satellite, weak AC cap
A7	2.0, 0.6/0.3	-3.0	0	Cap (AC), negative PV
S7	2.0, 0.3/0.3	-3.0	0.6	Cap (AC), negative PV, dipole
S8	2.0, 0.3/0.3	-1.5	0.6	Cap (AC), positive PV, dipole
A8	1.0, 0.6/0.3	2.0	0	Fission, 2 C satellites
A9	0.25-0.9, 0.6/0.3	2.0	0	Single stable C

TABLE 1. Initial vortex experiments. The Gaussian seamount parameters are given in the second column, and the vortex amplitude in the third. In all cases, the vortex radius was $r_0 = 0.3$. The fourth column indicates the separation between the vortex and seamount centres. The fifth includes comments on the results.

both x - and y - directions, but with a larger e-folding scale in x than y (recall that without β the field is otherwise rotationally invariant).

The initial vortex was specified with a Gaussian vorticity profile, $\zeta = A \exp[-(r/r_0)^2]$. Such vortices are frequently observed in freely evolving two-dimensional turbulence simulations (e.g. McWilliams 1990). Using such a vortex poses a difficulty with this model, whose integrated vorticity is necessarily zero (from periodicity). In practice, the model adds or subtracts a constant value of vorticity from the background to offset the vortex circulation. While not desirable, the background field was evidently too weak to affect the vortex-seamount interaction. An alternative choice is a vortex with a Gaussian streamfunction, which has zero integrated vorticity. However, the Gaussian streamfunction vortex is barotropically unstable and so evolves into a tripolar structure (e.g. Carton 1989); this obviously would alter the interaction with topography.

The vortex experiments are given in table 1.

The first cases are with a circular seamount. In experiments S1-S2, the vortex was initially aligned with the seamount. The only perturbations of this initial steady flow were due to numerical truncation errors. Both anticyclones and cyclones were stable, in agreement with the theory in §2.

In experiments S3-S4, the vortex was initially displaced from the centre of the circular seamount by a distance equal to the vortex e-folding radius. Note that this configuration pertains to the collision of a vortex with a seamount; now a portion of the initial flow is cross-isobath and all vortices accordingly evolve in time. The subsequent evolution is quite different for the cyclone and the anticyclone.

To understand why, it is useful to examine the evolution from the perspective of the potential vorticity. With an anticyclone on one seamount flank (case S3), the initial PV is dipolar because the topographic contribution is cyclonic. In the early evolution, the anticyclone draws fluid off the seamount, creating a cyclonic relative vorticity

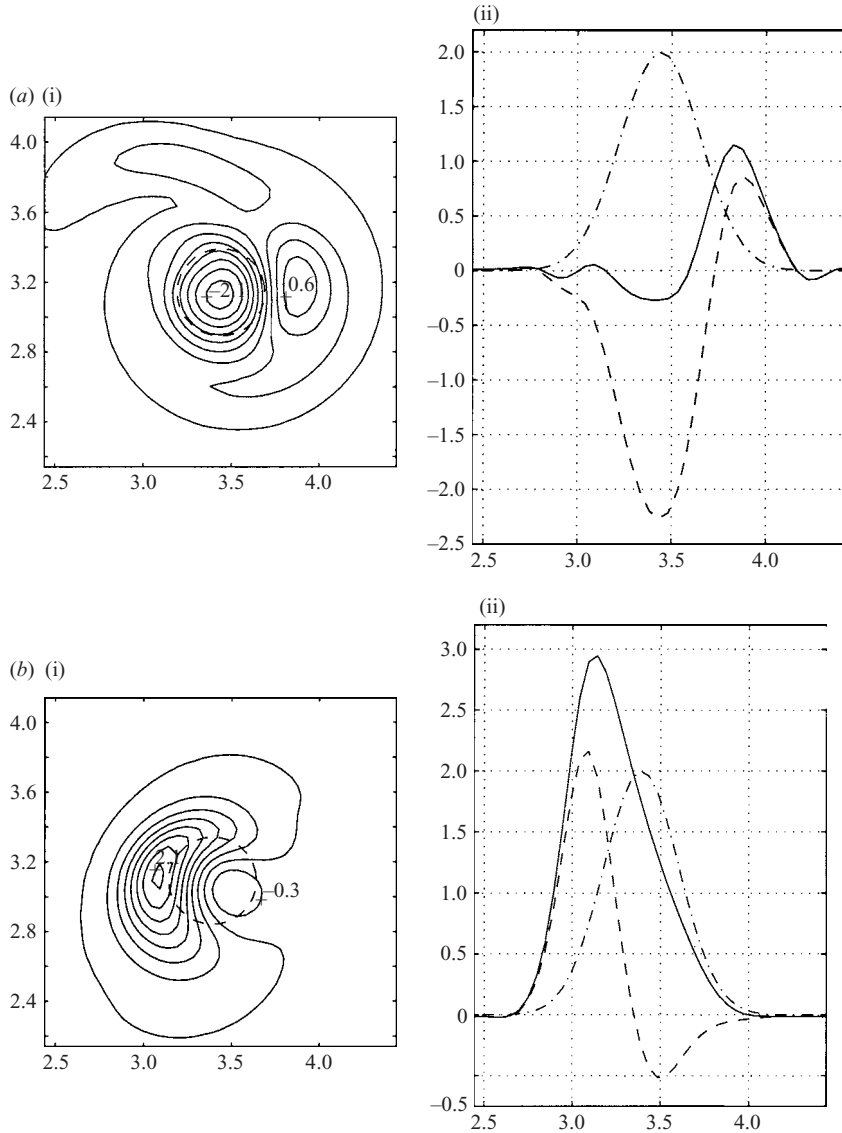


FIGURE 1. Experiments S3 and S4 with (a) an anticyclone and (b) a cyclone initially unaligned with a circular seamount. (i) The vorticity at a representative time after any initial adjustment has occurred. The vorticity contours are $\pm[0.3, 6, 0, \dots, 3]$. The dashed lines indicate the middle height ($h = 1.0$) isobath of the seamount. (ii) Slices in the x -direction of the vorticity (dashed line), topography (dash-dot) and their sum, the total PV (solid).

anomaly. The cyclone then shears off a portion of the anticyclone. The remainder of the anticyclone then shifts over the seamount centre, making an anticyclonic cap, while the ejected cyclone orbits clockwise around the seamount (i.e. with shallow water to its right-hand side). The relative vorticity at a later time and slices of the relative and total vorticity are shown in figure 1(a). Note that the seamount-trapped flow has a PV which is slightly negative.

With an initial cyclone (case S4), the PV is everywhere positive because both vortex and topographic contributions are positive. As might be anticipated from the

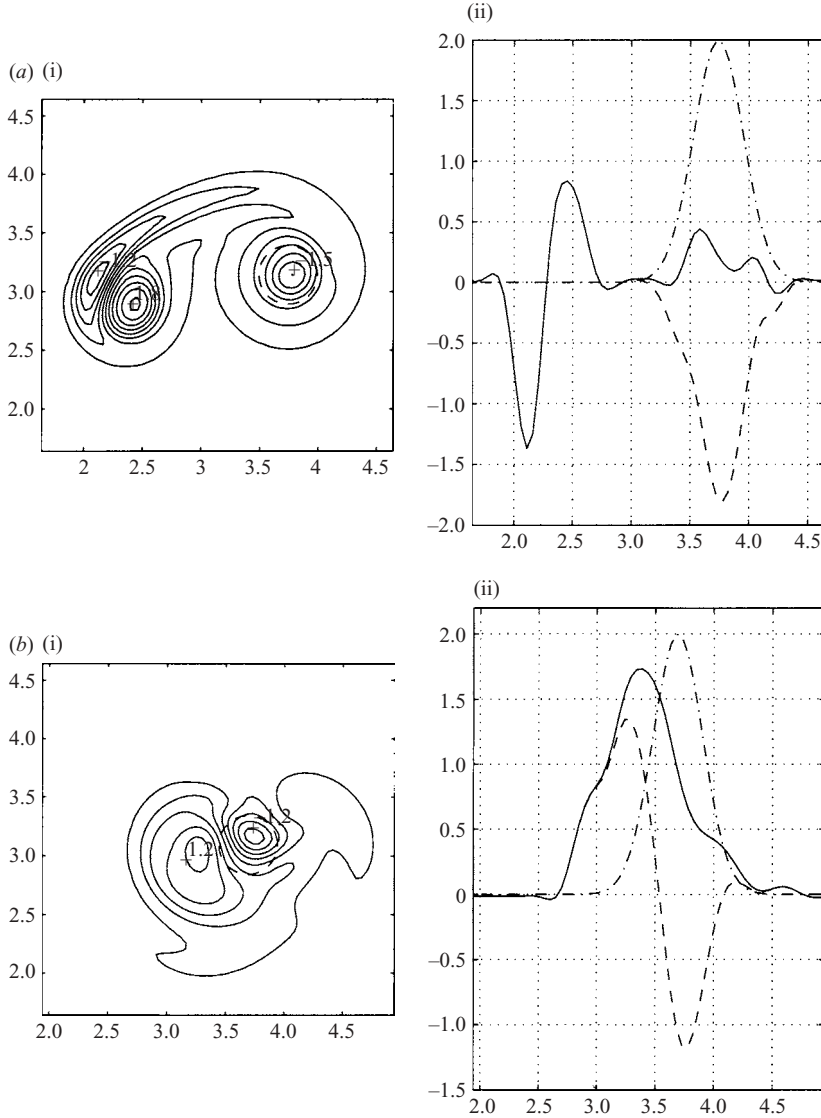


FIGURE 2. As in figure 1, but for (a) experiments S5 and (b) S6.

theoretical arguments, the cyclone never settles into a stationary configuration; rather it orbits clockwise around the seamount. Because of the flow contortions, a small anticyclonic relative vorticity anomaly occasionally is seen over the seamount summit (figure 1*b*), but the total PV remains positive everywhere (as it must).

In cases S5–S6, shown in figure 2, the vortices were displaced twice as far from the seamount centre. The subsequent evolutions were similar to those in the previous two cases, but somewhat more violent. Because the anticyclone in S5 covers less of the seamount, the cyclonic PV anomaly associated with the seamount is stronger, as is the relative vorticity of the fluid drawn off the seamount. The result is that the newly formed cyclone and a portion of the anticyclone translate away as a dipole. The final PV over the seamount in this case is slightly positive.

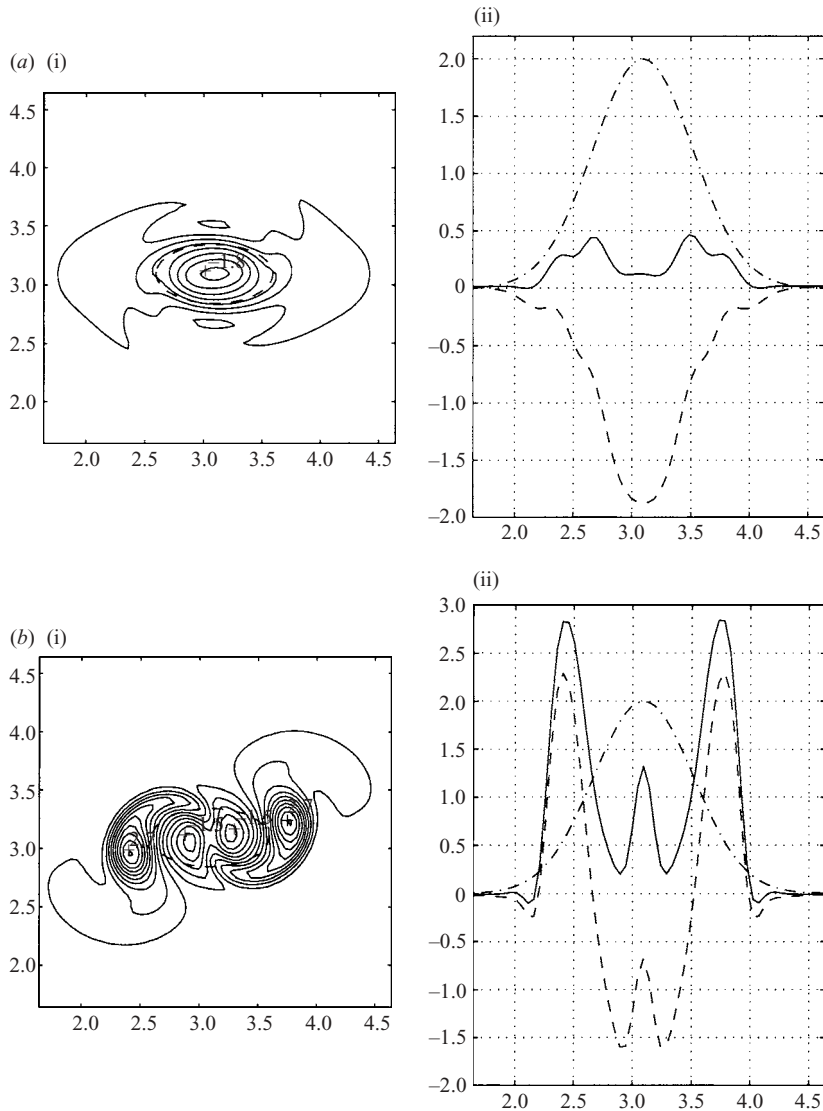


FIGURE 3. As in figure 1, but for (a) experiments A1 and (b) A2 with an asymmetric seamount.

With the initial cyclone (S6), the PV is again everywhere positive and the cyclone orbits the seamount. As in S4, an anticyclone forms over the seamount summit, but in S6 it is somewhat stronger. The evolution is otherwise very similar to S4.

Next we consider an asymmetric seamount; the seamount in all the A# cases had a zonal e-folding scale twice the meridional scale. As before, the (initially symmetric) vortices were placed over the seamount centre for the first two cases. The anticyclone A1 deformed so that its streamlines were approximately parallel to the isobaths and was stable thereafter (figure 3a). The final PV was weakly positive, although this depends on the relative amplitudes of vortex and seamount (see below).

The cyclone A2 in contrast fissions into two vortices after roughly 4–6 eddy turnover times. The two daughter vortices then orbit clockwise around the seamount. Over the

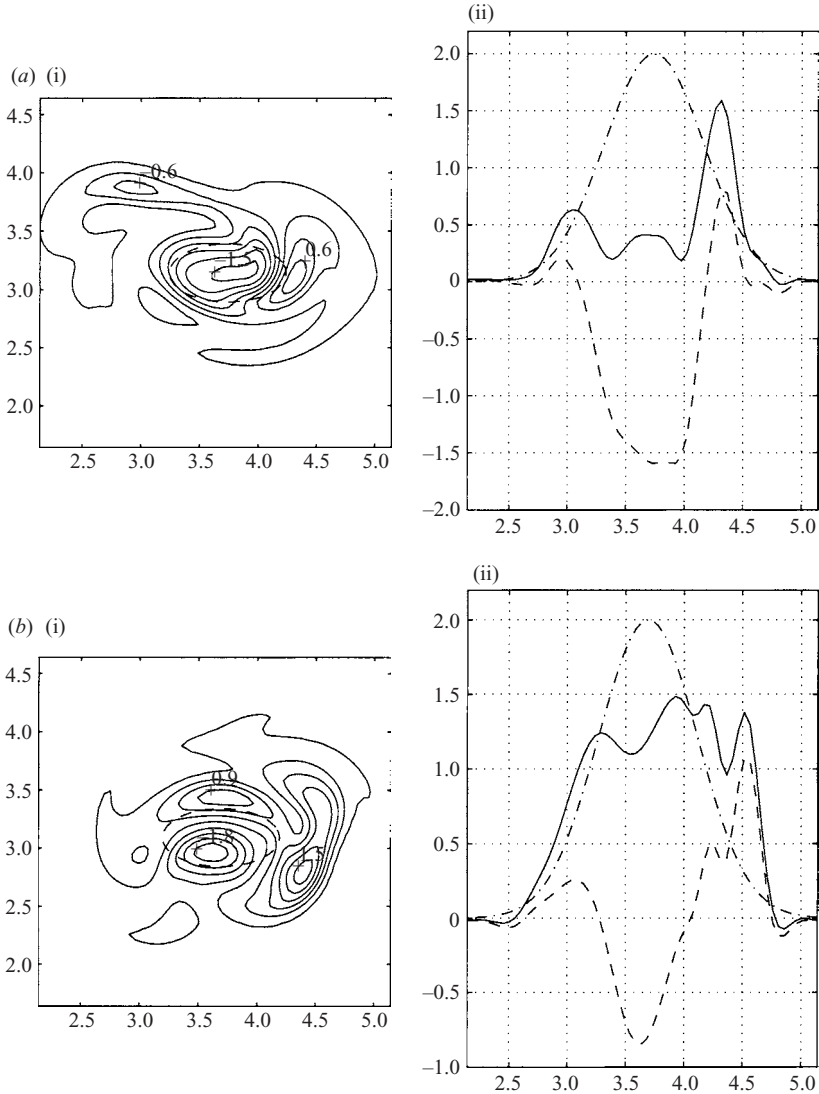


FIGURE 4. As in figure 1, but for (a) experiments A5 and (b) A6.

top of the seamount are two weak anticyclones (figure 3b); these alternately merge and separate as the outer cyclones precess. Note that the net PV over the seamount is positive.

In the four final A# cases, the vortex was displaced from the seamount centre and as with the symmetric seamount, the more extreme examples are those when the initial vortex is farther away. The anticyclone A5 draws fluid off the seamount, generating a cyclonic relative vorticity anomaly as in cases S3 and S5. As in S3, the cyclone remained near the seamount (after being sheared in two by the anticyclone) and thereafter orbited clockwise around the seamount. An anticyclonic cap with weakly positive PV was formed over the seamount (figure 4a).

The initial cyclone A6, on the other hand, undergoes a strongly time-dependent evolution, splitting into several pieces which then orbit clockwise around the seamount.

Some of the pieces merge thereafter, only to split again later on. As in A2, there is a region of negative relative vorticity at the seamount summit, though the total PV is still positive (figure 4*b*).

The details of the final state vary somewhat depending on the relative amplitudes of the vortex and the seamount. We consider now additional experiments in which we varied either the vortex or seamount amplitude (experiments A7–A9 and S7–S8 in table 1).[†] We consider the anticyclone first, and then the cyclone.

We return first to the anticyclone initially aligned with the seamount. As stated, the flow evolves only when the seamount is asymmetric. Experiment A7 (not shown) is like experiment A1 except that the anticyclone is 50% stronger. As in A1, the vortex deforms to make a cap over the seamount. However, where the final PV was weakly positive before, it is now weakly negative. To quantify the difference, we compare the PV integrated over a region bounded by an isobath ($h = 1.0$), normalized by the integrated topographic height. In A1, this ratio is about +0.15 whereas it is nearer –0.17 in A7. Perhaps significantly, the region where the PV is most negative in A7 is localized over the seamount summit; on the flanks, the PV is nearly zero. Thus, the sign of the final seamount PV can be either positive or negative.

With unaligned anticyclones, the final PV likewise can vary. In experiments S4 and S6, a cap formed over the seamount with a mean PV inside the $h = 1.0$ isobath of about 0.10. In experiments S7 and S8, the anticyclone is 50% stronger and 25% weaker, respectively (figure 5). In S7, the mean PV is around –0.17 and in S8 around 0.23. Decreasing/increasing the vortex amplitude further yielded similarly more positive/negative final PV.

With regard to the cyclone, varying the seamount (or vortex) amplitude produced in most cases similar results: unsteady evolution, with satellite vortices orbiting the seamount. The only case in which the outcome changed qualitatively was for the vortex aligned with an asymmetric seamount. In case A2, the vortex split into two smaller satellites; but fission need not occur if the seamount amplitude is smaller. In case A8, the seamount is half as high as in A2, and the vortex still splits in two (figure 6*a*). Fission also occurs with a seamount amplitude of 0.95. However, with an amplitude of 0.9 or less (case A9), the vortex does not break in two; rather, the vortex deforms into an ellipse whose major axis is perpendicular to that of the seamount (figure 6*b*). The vortex oscillates thereafter, so that the major axis swings left and right, but is otherwise stable. The end state thus depends sensitively on the seamount amplitude.

Why is this? As noted, the initial PV with a cyclone and seamount is everywhere positive. If they are aligned and the seamount is asymmetric, the asymmetry of the PV will depend on the relative contributions of the vortex and seamount. If the seamount dominates, the PV is similarly deformed. For flows without topography, it is known that a strong deformation causes fission (e.g. Dritschel 1986). The converse is that two like-signed vortices will merge if nearer than a critical distance. This is similar to what is seen here: if the single vortex is ‘stretched’ beyond a critical distance by the seamount, it splits.

To summarize, we observe distinctly different evolutions for the anticyclone and for the cyclone, in line with the theoretical considerations. Steady seamount-trapped flows are observed only in the former case. In the non-trivial cases in which the anticyclone

[†] Note that the effects of changing the seamount height or vortex amplitude are the same. From (1), scaling the seamount amplitude by a factor γ is the same as scaling the streamfunction by γ^{-1} and rescaling time by γ .

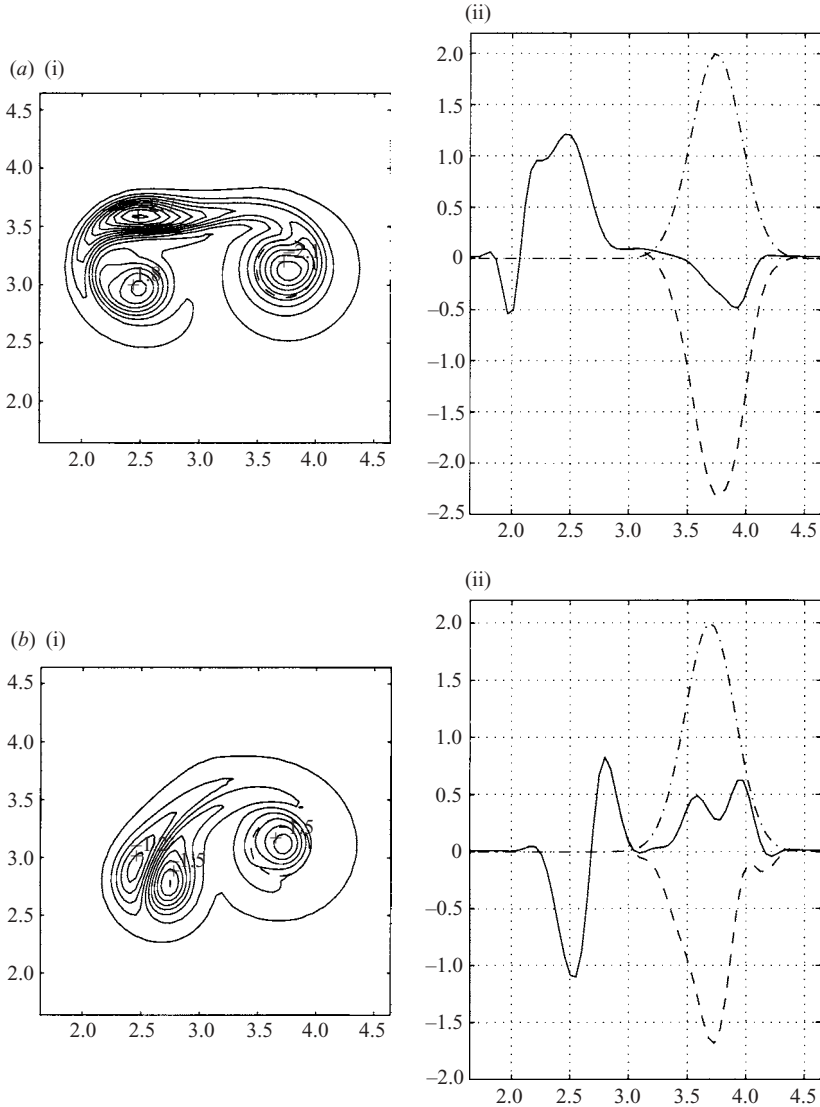


FIGURE 5. As in figure 1, but for (a) anticyclone experiments S7 and (b) S8.

was initially displaced from the seamount centre, a portion of the initial vortex would shift over the seamount centre (the rest being lost following an interaction with the fluid stripped off the seamount, of cyclonic vorticity). The PV of the trapped flow could be either positive or negative, supporting the presence of both maximum and minimum energy vortices.

The cyclone, which in combination with the seamount has a single-signed PV field, is trapped in the vicinity of the seamount, lacking an anticyclonic partner with which it can translate away. The resulting field can be strongly time-dependent, with the cyclone orbiting clockwise around the seamount and in some cases breaking into smaller vortices. A steady end state occurred only when the cyclone was initially aligned with a circularly symmetric seamount.

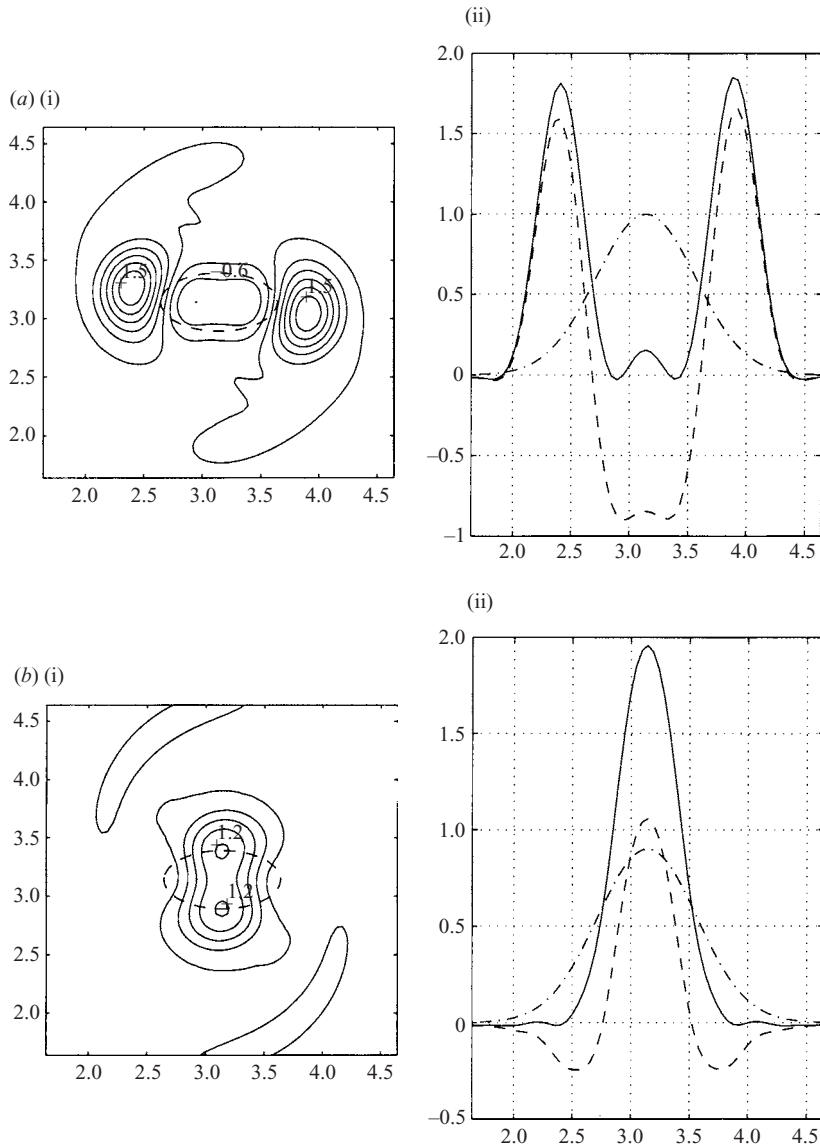


FIGURE 6. As in figure 1, but for experiments A8 and A9. The seamount height is 1.0 in (a) and 0.9 in (b). The dashed lines indicate the isobath at the seamount mid-height ((a) $h = 0.5$, (b) $h = 0.45$).

3.3. Turbulence

The vortex spin-down experiments are somewhat artificial in that a vortex is unlikely to materialize over a seamount (and particularly over its centre). A more realistic approach would be to have a flow in which vortices form independently and then interact with the topography. That is the goal of the last set of experiments, in which we begin with a random turbulent flow.

For these cases, we chose an initial flow with a specified wavenumber spectrum and random phases. As is well-known, the energy in such a turbulent, two-dimensional flow ‘cascades’ to larger scales (Kraichnan 1967; Kraichnan & Montgomery 1980).

Also well-known is that such spin-down experiments usually produce a field of long-lived vortices, in which like-signed vortices continually merge to form larger ones (e.g. McWilliams 1984). Many others have examined topographically trapped flows in the presence of freely evolving turbulence, most recently Merryfield, Cummins & Holloway (2001; and references therein). Our focus is somewhat different, on the mean PV over the seamount.

We took the initial spectrum to have zero energy at wavenumbers smaller than 14, and to vary as $\kappa^6/(\kappa + 2\kappa_0)^{18}$ at larger wavenumbers (here, κ is the total wavenumber and $\kappa_0 = 14$). The integrated kinetic energy was initially order one (yielding order one velocities). The energy cascade to larger scales proceeds rapidly at first, but more slowly later on. We let the adjustment proceed over an isolated seamount, and then examined the mean streamfunction by averaging during the slow adjustment period.

The results shown in figure 7 are representative. This seamount was like that in the previous (*A#*) experiments, with a zonal e-folding scale of 0.6 and a meridional scale of 0.3. The amplitude $H = 15$ was somewhat larger than the r.m.s. vorticity (which was 8.8 at $t = 10$ and 6.6 at $t = 40$), but smaller than that of many of the vortices which emerged from the initial flow.

The instantaneous vorticity at a time after the initial adjustment and the mean vorticity from the period $t = 10$ to $t = 80$ are shown in figure 7. The instantaneous field is dominated by vortices with amplitudes of 50 and greater and of various sizes. Mergers occur frequently and the background vorticity is strained and dissipated. The seamount can be seen as a perturbed anticyclone near the domain centre; however, the trapped vortex is clearer in the temporally averaged field (figure 7*b*).

The potential vorticity of the seamount-trapped flow is near zero, as can be seen in the slice shown in figure 8(*a*). Nevertheless, there are deviations which averaging has not removed, and these wiggles reflect vortices which have moved onto the topography (as seen in figure 8*b*). In the absence of the deviations, the seamount PV is nearly zero.

To examine both the vortex-induced fluctuations and the approach to a steady state over the seamount, we monitored the PV averaged over the upper half of the seamount (again normalized by the integrated topographic height) as a function of time. This is shown in figure 9 for four cases with seamounts of different heights and widths. Several points are apparent.

First, the time required to establish the mean circulation is greater if the seamount is tall and wide (e.g. figure 9*b*); for the shorter or narrower seamounts, the circulation sets up more quickly. What determines the adjustment time scale is unclear, but is probably related to the time required for the neighbouring vortices to strip away the fluid over the seamount summit. This evidently takes longer for taller and wider seamounts. Recall there is no dissipation here beyond that imposed by the wavenumber cutoff filter at small scales.

Secondly, the mean PV in all cases asymptotes to a value near zero. We recall that the seamount PV could be slightly positive or negative in the single vortex cases. Here, the ambient vorticity is zero, making it more likely that the seamount PV also approaches zero.

Lastly, the PV in all cases exhibits strong episodic deviations. These are due to vortex encounters with the seamount, even after the quiescent fluid has been stripped away. (Note the amplitudes of the fluctuations vary primarily because the integrated topographic height used for the normalization is different.) Curiously, the majority of these deviations are positive, reflecting that cyclones scale the seamount more

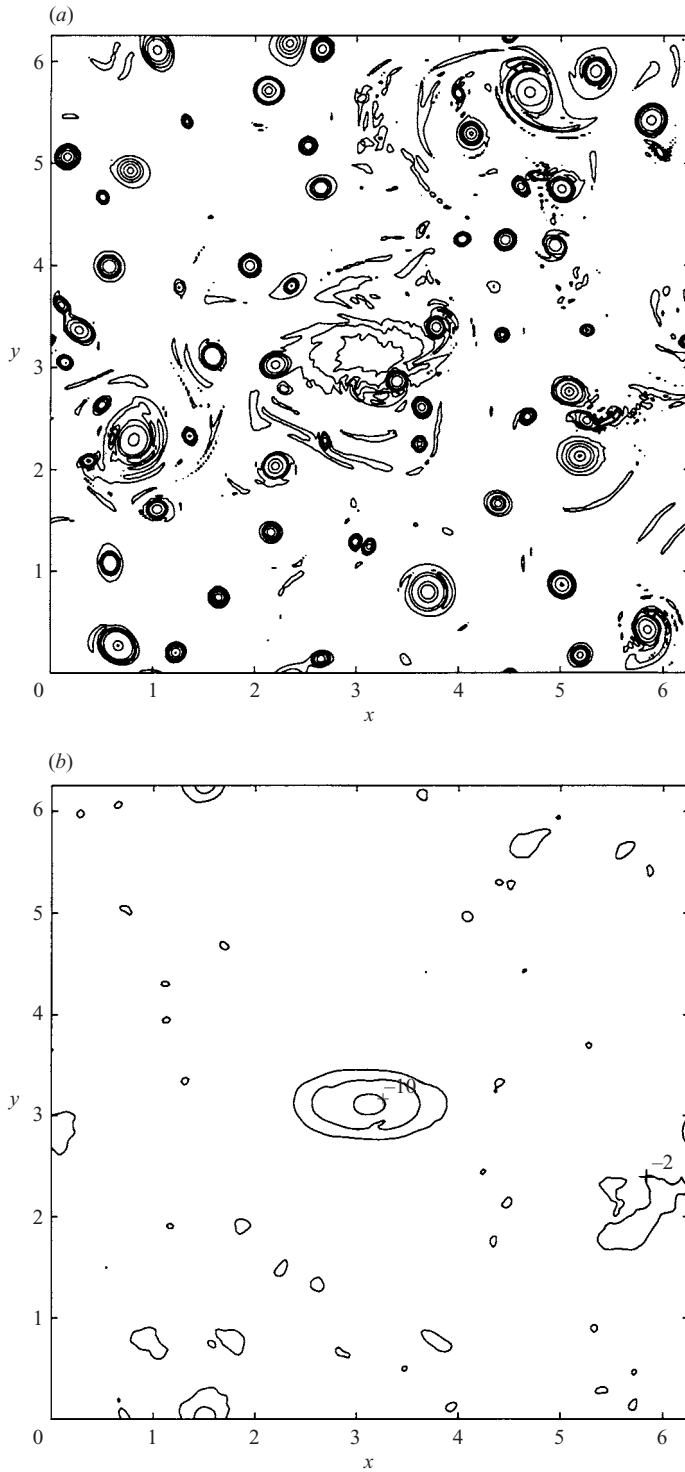


FIGURE 7. The (a) instantaneous and (b) mean relative vorticities from a turbulent spin-down experiment with an asymmetric seamount with the parameters $H = 15$, $r_x = 0.6$, $r_y = 0.3$. (a) $t = 20$; (b) $t = 10$ –80. The contour values, $\pm[2, 5, 10, 20, 50, 100]$, were chosen to highlight both the strong vortices and the weaker seamount-trapped circulation.

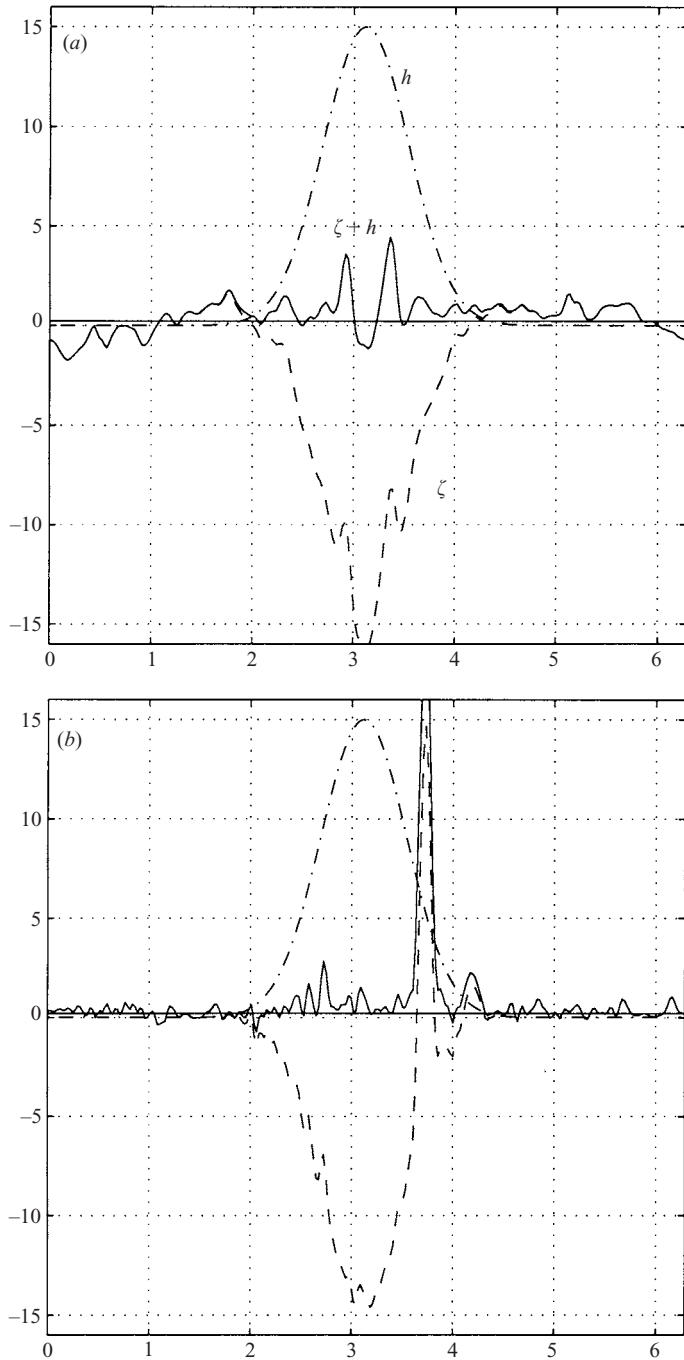


FIGURE 8. Zonal cross-sections of the relative (dashed), topographic (dash-dot) and total (solid) vorticities field from the turbulence run. (a) corresponds to the mean field and (b) to one instantaneous field at $t=40$.

frequently than anticyclones. The numbers of cyclones and anticyclones are roughly equivalent in these experiments, so the asymmetry is not due to an asymmetry in the background field.

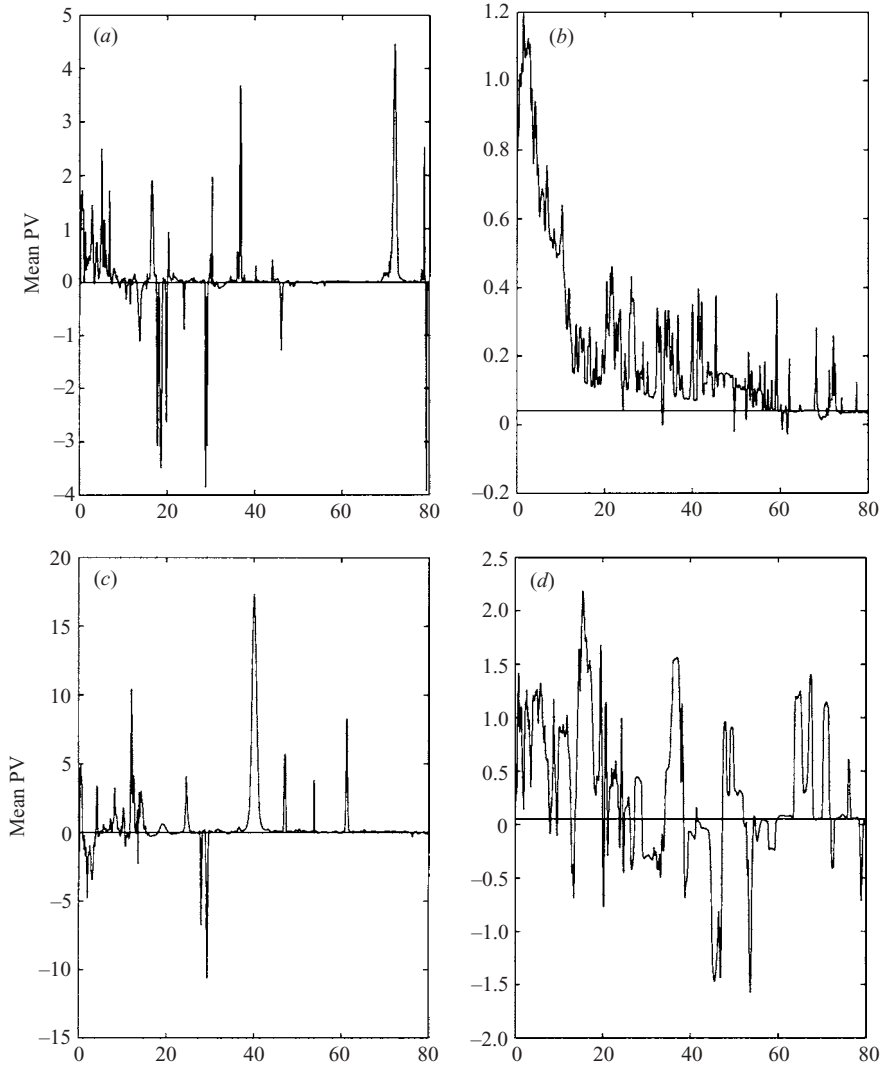


FIGURE 9. The PV integrated over the upper half of the seamount divided by the topography integrated over the same region, for several different seamounts. The seamount parameters are (a) $H = 15$, $r_x = 0.15$, $r_y = 0.075$; (b) $H = 15$, $r_x = 0.6$, $r_y = 0.3$; (c) $H = 3.75$, $r_x = 0.15$, $r_y = 0.075$; (d) $H = 3.75$, $r_x = 0.6$, $r_y = 0.3$.

Why would cyclones be favoured over the seamount? A tempting explanation is that they propel themselves up it, as cyclones are known to do up a linear slope (e.g. Carnevale, Kloosterziel & van Heijst 1991). Such self-propulsion occurs because the vortices perturb the mean PV gradient by advecting fluid across the isobaths. However, owing to the seamount trapped flow, the mean PV is near zero, so self-propulsion seems an unlikely explanation. Indeed, the reason for the asymmetry is unclear, but it appears to occur regardless of the seamount height or width.

4. Summary and discussion

We have studied the dynamics of vortices attached to an isolated topographic anomaly h , using both analytic variational methods and numerical simulations. The

topographic anomaly was assumed to have the same sign everywhere, but otherwise its shape is arbitrary.

According to a general variational principle, flows that maximize or minimize the energy in a set of isovortical flows are stationary and stable. In §2, we showed that a large number of different sets of isovortical flows contain such an extremal flow. Briefly, the theoretical results can be summarized as follows.

In every set of isovortical flows such that the PV-anomaly q everywhere has the opposite sign to the topographic anomaly h , a maximum energy flow exists. This flow is an attached vortex rotating in the same direction as, but faster than, the Taylor cap (i.e. an anticyclone over a seamount or a cyclone over a depression).

Also, in every set of isovortical flows such that q everywhere has the same sign as h and satisfies the inequality (12), a minimum energy flow exists. This flow is an attached vortex rotating in the same direction as, but more slowly than, the Taylor cap.

If the topography is circular, the conservation of angular momentum can be used to prove the stability of any vortex with a monotonic PV profile. This also includes vortices that rotate in the opposite direction as the Taylor cap (e.g. a cyclone over a seamount), although these are not minimum or maximum energy flows. Hence, the theory predicts that asymmetries in the shape of a seamount can destabilize an attached cyclone, but not an attached anticyclone.

These stability results were confirmed by numerical simulations. When a cyclone or an anticyclone was placed on top of a circular seamount, it remained stationary and stable. When a circular anticyclone was placed over an elliptic seamount, it first adjusted its shape, and the final flow was approximately stationary. By contrast, most circular cyclones placed over an elliptic seamount rapidly split into two vortices (unless the seamount was shorter than a critical height).

In the numerical experiments in which a vortex collided with the seamount, an anticyclonic cap was often formed. For the cases in which the offending vortex was anticyclonic, the resulting cap often had nearly zero PV, like a Taylor cap. However, instances in which the resulting PV was either positive or negative were also observed, depending on the strength of the initial vortex. We conclude that either maximum or minimum energy vortices can occur. When the initial vortex was cyclonic, the total PV was non-negative and the final flow was always time dependent.

In contrast to the range of possible final states in the vortex experiments, the turbulence experiments produced Taylor caps with near zero PV. They are presumably caused by the advection of ambient fluid, of zero mean PV, over the seamount.

Of course, most seamount-like structures in the ocean are asymmetric, and anticyclonic circulation should therefore be favoured. A possible example is the Zapiola Drift, an isolated topographic high occurring in an abyssal plain of the South Atlantic, where strong anticyclonic flow has been observed (Saunders & King 1995). Another example is the anticyclonic flow observed over the Fieberling Seamount (Kunze & Toole 1997). The PV anomaly of this flow was observed to be negative. Such a maximum energy flow cannot be explained by advection of ambient fluid. Kunze & Toole suggest that it is maintained by tidal rectification. The present results may help to explain the dynamic stability of this flow.

We should, of course, be cautious when comparing the present results for a simple barotropic model to the real ocean, which is stratified. However, it has been shown that the theoretical analysis in §2 carries over without much change to the three-dimensional quasi-geostrophic equation (Nycander 2003).

We are grateful to George Carnevale for useful comments. J. H. L. was partially supported by an ONR SECNAV scholarship while at the Woods Hole Oceanographic Institution, and by the Norwegian Research Council while in Oslo.

REFERENCES

- ARNOL'D, V. I. 1966 On an *a priori* estimate in the theory of hydrodynamic stability. *Izv. Vyssh. Uchebn. Zaved. Matematika* **54** (5), 3–5. (English transl. *Am. Math. Soc. Transl.*, Series 2, **79**, 267–269 (1969).)
- ARNOL'D, V. I. 1978 *Mathematical Methods of Classical Mechanics*. Springer.
- BENJAMIN, T. B. 1976 The alliance of practical and analytical insights into the nonlinear problems of fluid mechanics. In *Applications of Methods of Functional Analysis to Problems in Mechanics* (ed. A. Dold & B. Eckman). Lecture Notes in Mathematics, vol. 503, pp. 8–29. Springer.
- BRETHERTON, F. B. & HAIDVOGEL, D. B. 1976 Two-dimensional turbulence over topography. *J. Fluid Mech.* **78**, 129–154.
- BURTON, G. R. 1987 Rearrangements of functions, maximization of convex functionals, and vortex rings. *Math. Ann.* **276**, 225–253.
- BURTON, G. R. 1988 Steady symmetric vortex pairs and rearrangements. *Proc. R. Soc. Edin.* **108A**, 269–290.
- BURTON, G. R. & NYCANDER, J. 1999 Stationary vortices in three-dimensional quasi-geostrophic shear flow. *J. Fluid Mech.* **389**, 255–274.
- CARNEVALE, G. F. & FREDERIKSEN, J. S. 1987 Nonlinear stability and statistical mechanics of flow over topography. *J. Fluid Mech.* **175**, 157–181.
- CARNEVALE, G. F., KLOOSTERZIEL, R. C. & VAN HEIJST, G. J. F. 1991 Propagation of barotropic vortices over topography in a rotating tank. *J. Fluid Mech.* **233**, 119–139.
- CARNEVALE, G. F. & VALLIS, G. K. 1990 Pseudo-advective relaxation to stable states of inviscid two-dimensional fluids. *J. Fluid Mech.* **213**, 549–571.
- CARTON, X. 1989 In *Mesoscale/Synoptic Coherent Structures in Geophysical Turbulence* (ed. J. C. J. Nihoul & B. M. Jamart). Elsevier.
- DRITSCHEL, D. G. 1986 The nonlinear evolution of rotating configurations of uniform vorticity. *J. Fluid Mech.* **172**, 157–182.
- EMAMIZADEH, B. 2000 Steady vortex in a uniform shear flow of an ideal fluid. *Proc. R. Soc. Edin.* **130A**, 801–812.
- FILIPPOV, D. V. & YAN'KOV, V. V. 1986 Two-dimensional electron vortices. *Sov. J. Plasma Phys.* **12**, 548–552.
- FLIERL, G. R., MALANOTTE-RIZZOLI, P. & ZABUSKY, N. J. 1987 Nonlinear waves and coherent vortex structures in barotropic β -plane jets. *J. Phys. Oceanogr.* **17**, 1408–1438.
- GENIN, A., NOBLE, M. & LONSDALE, P. F. 1989 Tidal currents and anticyclonic motions on two North Pacific seamounts. *Deep-Sea Res.* **36**, 1803–1815.
- GREENSPAN, H. P. 1968 *The Theory of Rotating Fluids*. Cambridge University Press. 325 pp.
- HOGG, N. G. 1973 On the stratified Taylor column. *J. Fluid Mech.* **58**, 517–537.
- JOHNSON, E. R. 1978 Trapped vortices in rotating flow. *J. Fluid Mech.* **86**, 209–224.
- KRAICHNAN, R. H. 1967 Inertial ranges of two dimensional turbulence. *Phys. Fluids* **10**, 1417–1423.
- KRAICHNAN, R. H. & MONTGOMERY, D. 1980 Two-dimensional turbulence. *Rep. Prog. Phys.* **43**, 547–619.
- KUNZE, E. & TOOLE, J. M. 1997 Tidally driven vorticity, diurnal shear, and turbulence atop Fieberling Seamount. *J. Phys. Oceanogr.* **27**, 2663–2693.
- LACASCE, J. H. 1998 A geostrophic vortex over a slope. *J. Phys. Oceanogr.* **28**, 2362–2381.
- LODER, J. W. 1980 Topographic rectification of tidal currents on the sides of Georges Bank. *J. Phys. Oceanogr.* **10**, 1399–1416.
- MCWILLIAMS, J. C. 1984 The emergence of isolated coherent vortices in turbulent flow. *J. Fluid Mech.* **146**, 21–43.
- MCWILLIAMS, J. C. 1990 The vortices of two-dimensional turbulence. *J. Fluid Mech.* **219**, 361–385.
- MERRYFIELD, W. J., CUMMINS, P. F. & HOLLOWAY, G. 2001 Equilibrium statistical mechanics of barotropic flow over finite topography. *J. Phys. Oceanogr.* **31**, 1880–1890.

- NYCANDER, J. 1995 Existence and stability of stationary vortices in a uniform shear flow. *J. Fluid Mech.* **287**, 119–132.
- NYCANDER, J. 2003 Stable vortices as maximum or minimum energy flows. In *Nonlinear Processes in Geophysical Fluid Dynamics* (ed. O. U. Velasco Fuentes, J. Sheinbaum & J. L. Ochoa de la Torre). Kluwer.
- NYCANDER, J. & EMAMIZADEH, B. 2003 Variational problem for vortices attached to seamounts. *Nonlinear Anal.* **55**, 15–24.
- PATTERSON, G. S. & ORSZAG, S. A. 1971 Spectral calculations of isotropic turbulence: efficient removal of aliasing interactions. *Phys. Fluids* **14**, 2538–2541.
- SALMON, R., HOLLOWAY, G. & HENDERSHOTT, M. C. 1976 The equilibrium statistical mechanics of simple quasi-geostrophic models. *J. Fluid Mech.* **75**, 691–703.
- SAUNDERS, P. M. & KING, B. A. 1995 Bottom currents derived from a shipborne ADCP in WOCE cruise A11 in the South Atlantic. *J. Phys. Oceanogr.* **25**, 329–347.
- SHNIRELMAN, A. I. 1993 Lattice theory and flows of ideal incompressible fluid. *Russian J. Math. Phys.* **1**, 105–114.
- SOBOLEV, S. L. 1963 On a theorem of functional analysis. *Am. Math. Soc. Transl.* **34**, 39–68.
- TAYLOR, G. I. 1917 Motions of solids in fluids when the flow is not irrotational. *Proc. R. Soc. Lond. A* **93**, 99–113.
- VANNESTE, J. 1995 Explosive resonant interaction of baroclinic Rossby waves and stability of multilayer quasi-geostrophic flow. *J. Fluid Mech.* **291**, 83–107.
- ZIMMERMAN, J. T. F. 1978 Topographic generation of residual circulation by oscillatory (tidal) currents. *Geophys. Astrophys. Fluid Dyn.* **11**, 35–47.